

# TIME SERIES DEFORMATION ANALYSIS OF LUMPUR SIDOARDJO (LUSI) MUD VOLCANO USING INTERFEROMETRY SYNTHETIC APERTURE RADAR

PI0003

<sup>(1)</sup>T.P Sidiq, <sup>(2)</sup>Y. Aoki, <sup>(2)</sup>T. Kato, <sup>(1)</sup>H.Z. Abidin

<sup>(1)</sup> Geodesy Research Division of Institute Technology Bandung  
<sup>(2)</sup> Earthquake Research Institute of Tokyo University

## 1. INTRODUCTION

The combination of mud, steam, fluid, and gas erupted on 29 May 2006 in sub district Porong, Sidoardjo East Java (Fig 1). Term LUSI, stand for LUMpur (mud) SIDoardjo, was unofficially named to this eruption. This continuous eruption bring significant damage to the local social economy, infrastructures, and environmental. Milkov (2005) said that instabilities of mud volcano characteristics represent it as a geo-hazard.

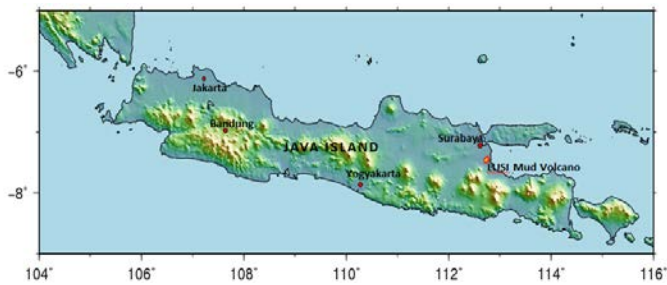


Figure 1 : Location of LUSI in Java Island

Four years after the first time observed eruption, about 12 million meter cubic of mud has been ejected. The mud is accommodated on about 620 hectare dike, some of the mud is released into the river near the dike and slowly shed the mud to the sea, around 10 km from the spill way. 14 villages buried by the mud, and about 30 thousand people should be relocated. The lost caused by LUSI reached 4 trillion rupiah (about \$US 4 billion) by the fourth year (Republika 2010). The lost is excluded from implicit lost due to degradation of transportation infrastructures, shattered of the local industries, and many other chain effects.

The rate and duration of LUSI mud volcano is very high and not usual (Davies, 2007). LUSI has contradictory behavior compared to most mud volcano exist in the present time. Among other mud volcano located in Java Island, none of them have equal effect with LUSI. Figure 2 shows how LUSI grows from 3.6 km<sup>2</sup> in August 2006 to 12 km<sup>2</sup> in December 2009. While the photographs (Fig 2) show the condition and main feature of the mud volcano. A dike had been made and has been maintained to prevent the mud from more massive mud covering.



(a)



(b)



(c)



(d)



(e)

**Figure 2: Land cover changing of LUSI mud volcano**

As the mud volcanoes are often associated with oil and gas activity (Milkov 2005), and so Porong area is one of an active area of oil and gas exploration/exploitation. LUSI itself is located only 150m from a gas exploration well called Banjar Panji-1. This well targeting gas on Kujung Formation within the East Java Basin. Mazzini et al. (2007) reports that the well drill up to 1828 meter. Davies et al (2007) proposed that LUSI is direct result of a high pressure fluid at depth with shallow sediments at a depth at which fractures can be initiated. However, Sawolo (2009) claimed that the drilling data and field facts do not support Davie's hypothesis.

Another mechanism had been proposed regarding LUSI mud volcano. Seismicity is known to have positive correlation with the mud volcano activity (Baciu 2005). Mazzini et al (2007), proposed that Jogjakarta earthquake which occurred on the 27<sup>th</sup> May 2006 was reactivated the Watukosek fault and triggered the LUSI mud volcano. Manga (2007) showed that the earthquake was not strong enough to triggered the LUSI. Moreover, the distance between Porong and the epicenter or the earthquake is too far to activate the eruption. Davies (2007) also notices that the preceded time by two days cannot trigger the eruption, because seismic liquefaction usually occurs during the earthquake-induced shaking sediment.

## METHODS

The ground deformation is mapped using differential interferometric synthetic aperture radar (DInSAR) method. This method provide a higher spatial resolution (some tens meter to below ten meter) at the centimeter level (Massonet and Feigl, 1998). Among the satellite based SAR data, ALOS PALSAR is used in this study. PALSAR used an L-Band microwave (23.6 cm), which has some advantages rather than the use of C-Band and X-Band. Takeuchi (2003) strongly suggest the uses of L-Band in tropical rain forest area like Indonesia to maintain good coherence value. In the LUSI case,

the eruption is surrounded by the rice fields and fish pond, and relatively high covered of vegetation.

More than 150 pairs of interferograms, spanning for different time period, are compute to measure the ground change around the LUSI area. These interferograms then be interpreted as a time-dependent range change using a least square inversion. In this study, the linear inversion methodology is used. Schmidt (2002) successfully performed a linear inversion to resolve the time-dependent subsidence and uplift.

## INSAR DATA PROCESSING

DInSAR uses at least two SAR images to create one ground displacement map, called two-pass DInSAR. The displacement is not a true horizontal and vertical displacement, but in radar system point of view called line-of-sight (LOS), which depend on the radar's look direction during the acquisition time. ALOS PALSAR orbit is set to allow two acquisitions observe the same place from same point every 46 days. PALSAR system also allows the data acquisition in different off-nadir angle that varies from 9.9° to 50.8°. Use of two SAR images that have same point of the data acquisition and same off-nadir angle is important in order to aim good result.

Level 1.0 ALOS PALSAR images used in the study. The images are divided into five frames, in both ascending and descending direction, span from June 2006 to December 2009 (Table 1). The temporal image is every one to three satellite revolution or about 46 to 138 days. However, the displacement occur in every 46 days is expected to be relatively small. The highest displacement rate inside and adjacent to the edifice (Abidin, 2008), is not expected to be revealed using InSAR method due to the low coherence. Images are paired in free combination, without any baseline or temporal constrain.

The data processing is performed using Gamma Software. Single complex look (SLC) image is first generated before the interferogram image. All images are processed without cropping, thus, one image will cover approximately 80x80 km. The images are preferred not to be cropped before the displacement map generated because the eruption area is relatively small and featureless. Interferogram processing is performed using 3 range looks, and 9 azimuth looks, which result roughly 30 meter of spatial resolution. An adaptive filter is applied in time domain during interferograms generation to increase the signal-to-noise ratio (Goldstein and Welner, 1998).

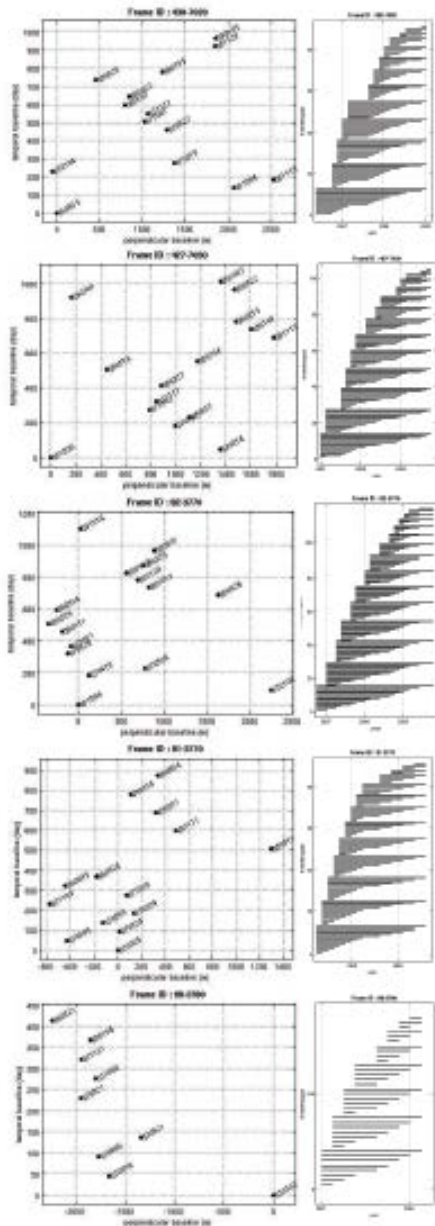


**Figure 3 : Data pairs for each satellite path**

Processing all data pairs is preferred rather than selecting them based on perpendicular baseline length. Figure 3 above show that the baseline can reach more than 2.5 km. Despite

the perpendicular baseline is very large, some parts of the images are still having good coherence. Large dataset is required to avoid the lack of data which can lead to underdetermined least square solution (Menke, 1989). However, coherence based masking is still applied on the computed displacement maps in order to maintain good quality of inversion analysis.

Interferogram is generated by subtracting phase difference between two images with a simulated phase of the terrain. A 3-arc-second (approximately 90 meter) SRTM digital elevation model (DEM) is used as the terrain height information. Linear absolute accuracy for SRTM DEM is less than 16 meter (Rodriguez, 2005; Berry et al., 2007), which result the phase error due to topography that can be neglected though for long baseline data pairs (Fukushima, 20009). ALOS PALSAR images come with good orbital information with 1 meter accuracy. However, there still error caused by orbit inaccuracy which is subtracted from calculated displacement map using estimation of 2-dimension quadratic model phase function.

Atmospheric errors are mainly caused by ionospheric and tropospheric influences. The ionospheric influences are frequency-dependent which is hard to be modeled. While the tropospheric influences is usually divided into hydrostatic, wet and liquid components (Hanssen, 2001). The hydrostatic component is mainly related to refractive index of air pressure (e.g. altitude) and wet delay on the water vapor pressure (Jehleet.al, 2008). The hydrostatic component which has height dependent characteristic is reduced using linear model consisting a phase constant and phase slope. While the hydrostatic component is reduced, other components that lead to several centimeters of error are still remaining on the displacement map (Fukushima, 2009).

### LEAST SQUARE INVERSION

We performed least square inversion to reveal the time series of change in range direction. The total deformation in a point during a period ( $d$ ) that divides into  $n$  discontinuous observation is simply denoted by,

$$m1+m2+...+mn=d$$

Where  $m1$  through  $mn$  are the incremental range changes, or range change during a sub-period (Fig ...). A matrix equation can be arrange once we have many observation of  $d$  as below,

$$\mathbf{Gm}=\mathbf{d}$$

$\mathbf{m}$  is a vector contains deformation in all sub-period, and the total deformation during a period of observation is arrange in matrix  $\mathbf{d}$ . Matrix  $\mathbf{G}$  is the design matrix, contain only two possible number, one or zero. The equation can be described schematically in Figure ...

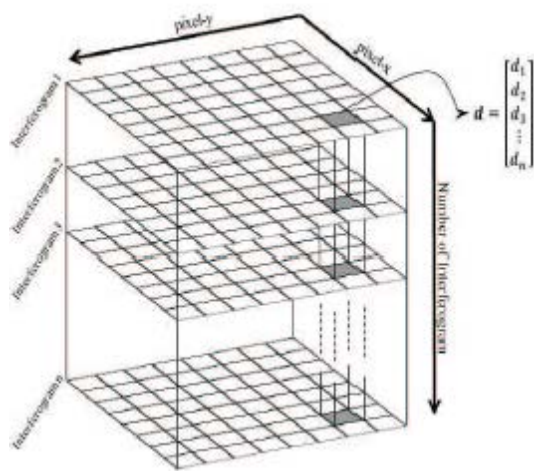


**Figure 4 : Idea of the Time Series Analysis**

The time series range change  $C$  is constructed by summing the incremental range change above. Thus,  $C$  can be arranged as follow,

$$C = \begin{bmatrix} m_1 \\ m_1 + m_2 \\ m_1 + m_2 + m_3 \\ m_1 + m_2 + m_3 + m_4 \\ \vdots \end{bmatrix}$$

Matrix design  $G$  is formed from temporal distribution of SAR images. For  $n$  number of SAR images, which form  $m$  set of interferogram, a  $1 \times n$  vector contain acquisition date arranged in series ( $L$ ), and a  $2 \times m$  matrix of master and slave date ( $H$ ) can be arranged. Once this matrices are arranged, design matrix  $G$  can also be .

The inversion describes above can only be implemented on the same location that is represented by pixel position. Thus, all interferograms should have common spatial reference to ensure that every pixel represent the same location. Inversion process is repeated for each pixel on the image. A three dimension matrix  $M$  is resulted by arranges each vector  $m$  into its original position in pixel coordinate.  $M_{ijk}$  represent incremental range change in  $k$  time, in pixel  $(i, j)$ .

Number and temporal distribution of the interferogram will determine the quality of the data resolution, as well as the inversion model. Using the free combination of SAR images, leads to big difference between the number of SAR images ( $n$ ) and the number of interferogram, with ratio  $2:(n*(n-1))$ . However, the low coherence pixel should be excluded from the inversion process. 0.35 coherence cutoff is implemented in this study. The average coherence value in the eruption area is relatively bad because of its land cover and temporal resolution in some interferograms. The data set in each pixel is only inverted if only the data lost less than 30% to void underdetermined solution.

The time series temporal resolution is determined by the

image acquisition rate. Since the acquisition rate in this study is not constant, we perform a piecewise cubic interpolation to generate equally time resolution of the final time series. The same process is performed on the GPS data comparison, as well as the subsidence vector decomposition process. Despite the interpolation process can provide denser time series, it will not increase the quality of the inversion model.

As radar system can only measure deformation in LOS direction, decomposition is needed when comparing interferograms with GPS data. A LOS displacement with components  $d_u, d_e, d_n$  mean deformation in up, east and north direction respectively, is a function of radar incidence angle, and heading direction.

Using both ascending and descending observation give a possibility to decompose two of three displacement vector (Hanssen, 2001).

### TEMPORAL SMOOTHING

As a smooth final time series is expected, a smoothing constrain is implemented on data analysis. This smoothing will minimize the time-dependent errors, including atmospheric artifact. The finite difference is performed to approximate the smoothing factor  $\gamma$ . The smoothing constraint assumes a small deformation occur during a short period of time (Schmidt, 2003). The smoothing factor is already implemented at the inversion step by augmenting the linear equation into matrix design  $G$  and matrix  $d$ .

$\gamma$  controlled the smoothness, where  $\gamma=0$  means no smoothing is performed, and the higher the gamma, the smoother the model will be. But setting gamma too large will eliminate the deformation signal itself. Thus, gamma value determination must be taken carefully. We applied different gamma value for each frames. Each gamma value is determined by finding the maximum curvature from a function of roughness and residual.

Below is an example of L-Curve for path 91\_3370

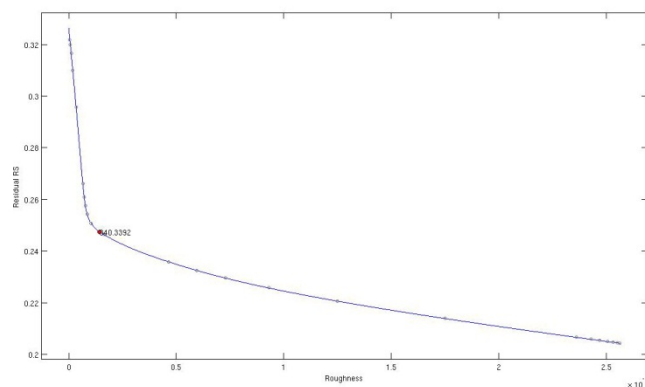


**Figure 5 : Example of L-Curve (path 91\_3370)**

### RESULT

In general, the deformation could be revealed very well using InSAR method in the case study area. An ellipsoidal pattern is clearly visible from the interferograms (Fig 6) with the

subsidence rate in the first 8 months is much greater than after. The maximum deformation reach ~32 cm from June to October 2006, while the total maximum deformation reach ~60 cm in more than three years. An uplift pattern is observed in the north side of the eruption. The uplift is considered as a buoyancy effect.

Another deformation pattern is also observed in the north east direction of the main crater with maximum LOS deformation reach ~30 cm in more than three years. The cause of this phenomenon still needs further analysis, which is not included on this study.

The GPS measurement shows much lower value in a point adjacent to the center of the crater (Fig 7). Smoothing factor is expected caused this significant difference. Although the smoothing process reduce some errors in the processed interferograms, but it also effect the signal itself, and specially the big signal occur in the first months in this case.

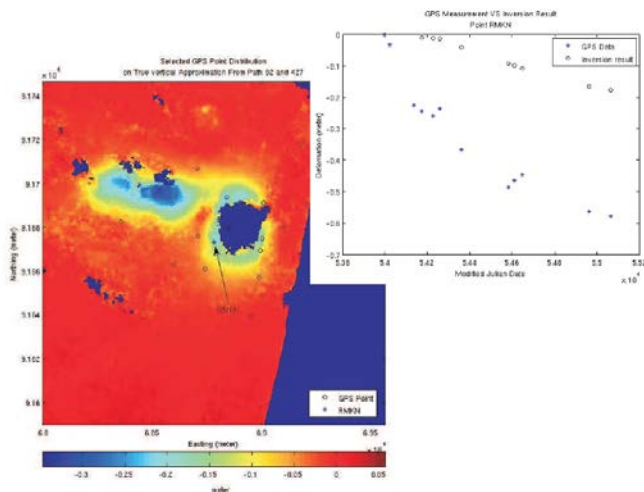


Figure 6 : GPS and InSAR data comparison

## CONCLUSION

InSAR method reveals a big deformation in ellipsoidal form, cover approximately 3km x 6km (18km<sup>2</sup>). The ellipsoidal form is confirmed by the fact of how the cracks appear around eruption area (Fig 8). Two different pattern of subsidence is clearly visible. Deformation outside the main eruption has almost similar rate with the main eruption, but remain unexplained

Linear inversion perform well although no further parameterize method was used. Smoothing factor that is used on this study caused some important signal lost. Because of that, the study about smoothing factor determination is still needed to get the better result.

The time series analysis also reduces the atmospheric error, and can be used as a good tool in large data set interpretation. A better understanding of the temporal variation can be given by the method, although a large data set is needed to perform good analysis.

## PLAN IN THE FUTURE

As the smoothing factor has not well performed in this case, we plan to use other temporal filtering methods. The temporal filtering becomes important issue because the atmospheric error varies through time. Temporal filtering can reduce the atmospheric error very well, and also provide better time series analysis.

More GPS data comparison will also be done in the future. Only one GPS point out of 52 GPS points is compared with the InSAR data processing result right now.

The final goal to achieve is the source modeling. Right now, many scientists try to model the source of the mud volcano using many data, but none of them had modeled it using InSAR data. As the data processing finish, a paper is also planned to be published in the near future.

## JOINT WORK

This research is a joint work between Earthquake Research Institute (ERI) of Tokyo University, and Institute Technology Bandung through JICA program. The pre-result of this research had been presented in poster session of AGU meeting las December, San Francisco USA.

## REFERENCES

- Abidin H. Z, R. J. Davies, M.A. Kusuma, H. Andreas, T. Deguchi}, Subsidence and uplift of Sioardjo (East Java) due to the eruption of the Lusi mud volcano (2006-present), Environmental Geology, 2008
- Takeuchi, Y. Oguro, A comparative study of coherence patterns in C-Band and L-Band Interferometric SAR from tropical rain forest areas, Advanced Space Res Vol. 32 p.2305-2310, 2003
- Schmidt D, A, Burgmann, R, Time-dependent land uplift and subsidence in the Santa Clara valley, California, from a large interferometric synthetic aperture radar data set, Journal of Geophysical Research Vol 108, p. 1-13, 2003

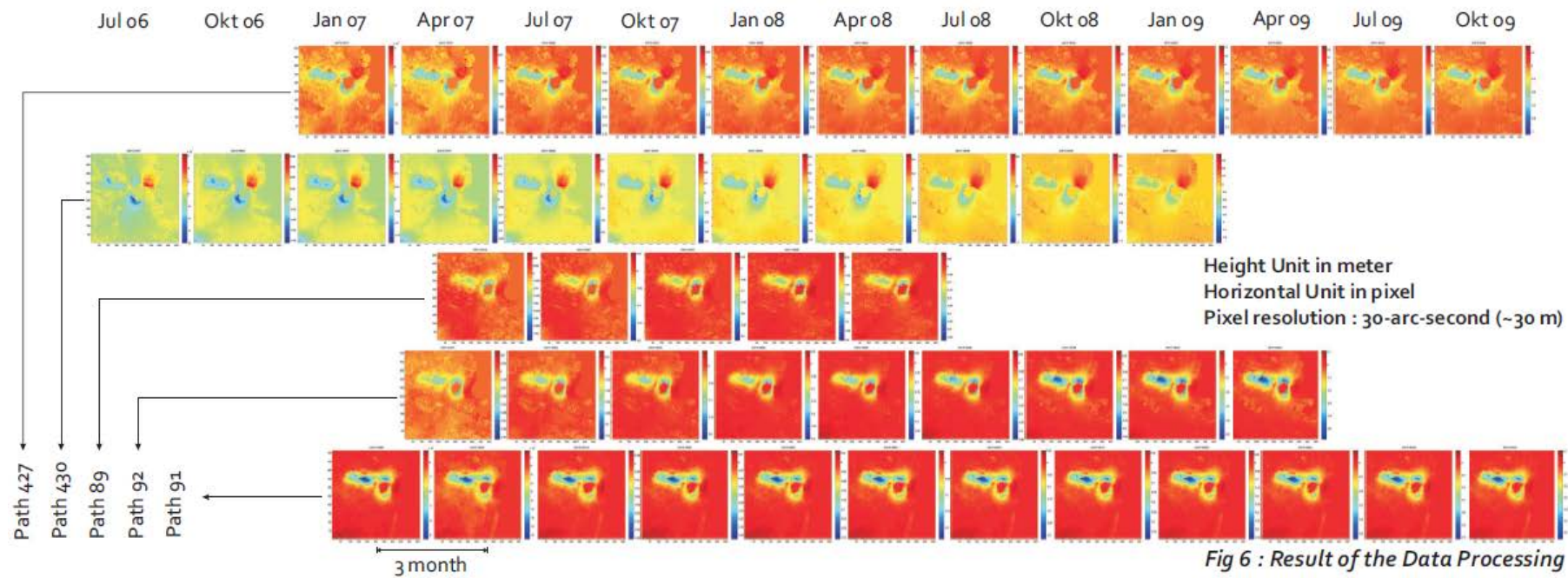


**Figure 7 : Result of the data processing**